

# LoL-NMPC: Low-Level Dynamics Integration in Nonlinear Model Predictive Control for Unmanned Aerial Vehicles

Parakh M. Gupta, Ondřej Procházka, Jan Hřebec, Matej Novosad, Robert Pěnička, Martin Saska

**Abstract**—In this paper, we address the problem of tracking high-speed agile trajectories for Unmanned Aerial Vehicles (UAVs), where model inaccuracies can lead to large tracking errors. Existing Nonlinear Model Predictive Controller (NMPC) methods typically neglect the dynamics of the low-level flight controllers such as underlying PID controller present in many flight stacks, and this results in suboptimal tracking performance at high speeds and accelerations. To this end, we propose a novel NMPC formulation, *LoL-NMPC*, which explicitly incorporates low-level controller dynamics and motor dynamics in order to minimize trajectory tracking errors while maintaining computational efficiency. By leveraging linear constraints inside low-level dynamics, our approach inherently accounts for actuator constraints without requiring additional reallocation strategies. The proposed method is validated in both simulation and real-world experiments, demonstrating improved tracking accuracy and robustness at speeds up to  $98.57 \text{ km h}^{-1}$  and accelerations of  $3.5 \text{ g}$ . Our results show an average 21.97 % reduction in trajectory tracking error over standard NMPC formulation, with *LoL-NMPC* maintaining real-time feasibility at 100 Hz on an embedded ARM-based flight computer.

## SUPPLEMENTARY MATERIAL

Webpage: <https://mrs.fel.cvut.cz/lol-nmpc>

## I. INTRODUCTION

UAVs have garnered considerable research interest due to their remarkable versatility as they can take off and land vertically, loiter at any 3D position, and execute high-speed manoeuvres with extreme agility. When outfitted with a variety of scanning sensors, UAVs have proven effective in applications such as search-and-rescue [1], oil-spill and fire-perimeter monitoring [2], radiation source tracking [3], [4], infrastructure inspection [5], [6], and aerial coverage scanning [7]. The combination of their versatile capabilities and increasing autonomy is enhancing the efficiency in these operations.

For nearly all of these applications, UAVs are operated at moderate speeds, without pushing them to their performance limits. In contrast, autonomous drone racing [8] challenges both the hardware and autonomy capabilities of these vehicles, yet it only serves as a benchmark scenario for applications such as search-and-rescue. Nevertheless, all the aforementioned applications that use UAVs as autonomous flying sensors can benefit from fast, agile flight, especially with the advent of high-speed cameras and other fast sensors.

The authors are with the Multi-robot Systems Group, Faculty of Electrical Engineering, Czech Technical University in Prague, Czech Republic (<http://mrs.felk.cvut.cz/>). This work has been supported by the Czech Science Foundation (GAČR) under research project No. 23-06162M, by the European Union under the project Robotics and Advanced Industrial Production (reg. no. CZ.02.01.01/00/22.008/0004590) and by CTU grant no SGS23/177/OHK3/3T/13.

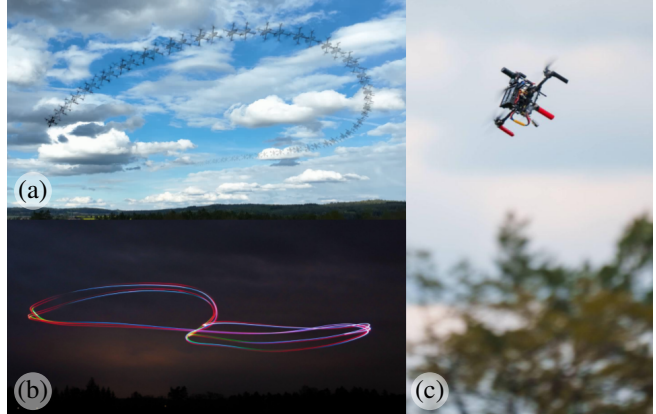


Fig. 1: Illustrative stills from real-world experiments: (a) UAV in flight, (b) long-exposure shot of its trajectory at night, and (c) UAV used in the experiments.

However, when UAVs operate at high speeds and execute agile manoeuvres, the risk of significant deviations from planned trajectories (e.g., during inspection missions) increases, potentially jeopardizing the mission by missing the desired position for data collection or by colliding with the environment. To address this challenge, this paper focuses on onboard control aimed at following a desired trajectory with minimal deviation, that is, to reduce trajectory tracking error, even for agile and fast trajectories (see Fig. 1).

Trajectory tracking is a challenging task due to nonlinear UAV dynamics, propulsion and aerodynamic modeling inaccuracies, actuator dynamics, and delays in state estimation and control loops. At the same time, the desired trajectories can either consider the feasible but computationally expensive full-scale dynamics model [9], or a simplified point-mass model which can be quickly computed onboard [10], but is rather challenging to track due to its partial dynamic infeasibility. To improve the tracking performance, the UAV systems [11], [12], [13] often rely on a high-level controller that runs on a companion onboard computer and commands a separate low-level controller which runs on a flight-controller unit. However, the interaction between the high-level and the low-level controller can cause mismatches, especially in agile flight, and thus complicate precise tracking. Pushed to their actuator saturation limits, the UAVs can generate larger tracking errors by either lagging behind, overshooting or cutting the corners and due to this cause a collision with any obstacle that the trajectory was planned around. To fly at the limits of the platform, the high-level controller needs to model the dynamics of the UAV as close to the real dynamics of the UAV as possible.

Existing works on high-level control can be broadly categorized into predictive controllers, such as Nonlinear Model Predictive Controller (NMPC) [14], and non-predictive controllers, including Differential-Flatness-Based Controller (DFBC) [15] and Proportional Integral Derivative (PID). While non-predictive controllers [15] are computationally efficient, they rely on feasible trajectories to maintain low tracking errors and often fail to account for the full UAV dynamics. In contrast, predictive controllers like NMPC [14] leverage modelling of the dynamics to track even partially infeasible trajectories, such as those presented in [10]. This is also why the research on NMPC has primarily focused on improving UAV dynamics modelling [14]. Standard NMPC formulations use single-rotor thrust as the control input [11], while others rely on propeller acceleration [16]. Additional studies have explored hybrid approaches, integrating NMPC with adaptive control [17], and investigated the impact of low-level and inner-loop controller choices [13]. However, in many cases, the control inputs required by the low-level controller differs from those modelled within NMPC [9], [13]. Furthermore, to the best of our knowledge, the true dynamics of low-level controllers have either been entirely neglected in NMPC formulations or inaccurately approximated as first-order systems [14].

To this end, our work introduces a novel NMPC which, apart from the standard quadrotor model, also considers both the dynamics of the low-level PID flight controller (that is used in many quadrotor flight stacks such as [12], [11]) and the dynamics of the motors themselves. By leveraging the motor mixing matrix of the low-level flight controller, we accurately model the actuator rise-time dynamics, including PID and motor effects, to enforce both collective and single-rotor constraints directly, and thereby eliminate the need for reallocation strategies for any throttle input. By modelling the low-level dynamics, the proposed *LoL-NMPC* addresses the model mismatch when using low-level flight controller together with high-level NMPC control.

We demonstrate the effectiveness of our approach in enhancing trajectory tracking performance while maintaining computational efficiency in both simulation and real-world experiments. The *LoL-NMPC* runs at 100 Hz on a small ARM-based flight computer, with only a 56 % increase in computational time compared to the standard NMPC formulation. Our method has been tested across various trajectory types, consistently delivering improved performance. The *LoL-NMPC* outperforms standard approaches, achieving an average 21.97 % reduction in trajectory tracking error while operating outdoors at speeds of up to  $98.57 \text{ km h}^{-1}$  and accelerations reaching 3.5g.

## II. RELATED WORK

For agile and high-speed flight, choice of the type of controller has been a contested topic due to various advantages and disadvantages of each type of controller. Among non-predictive controllers, the geometric SE3 controller, proposed in [15], is widely used for agile flight throughout the literature and has been very successful in real-world applications.

However, its non-predictive nature prevents it from performing multi-goal optimisation or accounting for actuator saturation. Predictive controllers were, until recently, constrained by onboard computing, but advances in commercial toolboxes now enable real-time high-speed control [18] [19], [20]. Predictive controllers offer the advantage to account for actuator saturation limits and the physical constraints of the platform using the dynamics model of the UAV. As a result, they handle infeasible trajectories more effectively than non-predictive controllers [13]. However, to fly at the limits of the platform, the dynamics model inside the NMPC needs to be as close to the real dynamics of the UAV as possible, and including the dynamics and delays originating from the low-level controller becomes crucial to achieve this goal.

Researchers have focused on identifying and modelling the dynamics of the UAV with increasing detail, for example, by studying aerodynamic effects and propulsion effects. A seminal work from the authors of [21] showed that the model of a quadrotor, without the aerodynamics drag, was differentially flat if position and heading were considered as outputs. Controllers built on this model have been shown to be able to track trajectories with high accuracy and speed. However, there has been significant research into modelling drag as a first-order effect, and using blade element theory has led to notable performance improvements in both predictive and non-predictive controllers [22], [23]. Authors of [24] showed that the dynamics of the UAV remain differentially flat when drag is modelled as a first-order system. Identification of such models has been a challenge for traditional methods, and to remedy this, neural-network based approaches have also been presented for identifying and modelling the aerodynamic effects and motor dynamics without increasing the computation time [25]. Another key aspect of the UAV dynamics is the propulsion system, and the authors of [26] showed that the use of motor modelling can improve the performance of the controller. Similarly, choice of input has shown to be a key factor in modelling and [16] discussed the derivation and use of acceleration of the propellers as an input to the NMPC for improved performance on tilt-hex and tilt-quadruped UAVs. Therefore, we tackle this by including the drag characteristics, motor dynamics in our model to improve the tracking performance of the UAV.

The work presented in [24] demonstrated how a DFBC can account for drag effects and track trajectories with high accuracy and speed. For similar agile and high-speed flight, the authors of [13] showed that DFBCs offered 100 times lower compute time in comparison to NMPC controllers, and provided better performance than the NMPC in case of translational disturbances such as external forces and mass mismatch. However, in their research, the NMPC controllers far outperformed the DFBC controllers in trajectory tracking and showed much lower crash rates in cases of rotational disturbances such as centre-of-gravity bias or external moment as well as when tracking infeasible trajectories. The DFBC is shown to primarily suffer due to the inability to account for saturation limits of actuators and physical limits of the platform, as opposed to the NMPC. Work in [13] also

discussed solving this problem by allocating control using a Quadratic Programming (QP) solver. Prior to this, [26] presented that the use of an iterative mixing scheme improves position tracking performance on a UAV when actuators are saturated or prevented from saturation. We propose a novel integration of low-level dynamics and linear constraints on the intermediate state which allows us to eliminate the need for reallocation strategies for any throttle input. Finally, while a significant amount of research has been focused on modelling propulsion and aerodynamic effects, [13] highlighted that the choice of inner-loop controller is more crucial than modelling aerodynamic effects, as the performance yields are much higher with Incremental Nonlinear Dynamic Inversion (INDI)-coupled control schemes. This was further proven by work in [27], as the researchers pushed the limits of DFBC by combining it with INDI to achieve high-speed flight of up to  $12 \text{ m s}^{-1}$  at sub-10 cm accuracy. Another key area of mismatch was highlighted by [14], where it was discussed that in a cascaded control architecture, inner-attitude controllers are usually approximated as first-order systems although they are second-order systems in reality, and the disturbances accrued from this assumption in modelling require the high-level controller to reject these deviations as disturbances during high-speed flight. Therefore, we propose a novel method in the next section which bridges the gap between the low-level controller dynamics and the high-level controller dynamics incorporating rate controller dynamics into the NMPC formulation.

### III. PROBLEM FORMULATION

To understand the modelling problem, we first need to discuss the UAV dynamics, control input selection, and the standard UAV model within an NMPC framework.

#### A. Standard UAV model

The UAV state is represented by  $\mathbf{x} = [\mathbf{p} \ \mathbf{q} \ \mathbf{v} \ \boldsymbol{\omega}]^T$  which comprises of position  $\mathbf{p} \in \mathbb{R}^3$  and velocity  $\mathbf{v} \in \mathbb{R}^3$  in world-frame, unit quaternion rotation  $\mathbf{q} \in \mathbb{SO}(3)$ , and body rates of the aircraft (angular velocity of aircraft in body-frame)  $\boldsymbol{\omega} \in \mathbb{R}^3$ . The dynamics of the UAV can be summarized as

$$\dot{\mathbf{p}} = \mathbf{v}, \quad (1a)$$

$$\dot{\mathbf{v}} = \frac{\mathbf{R}(\mathbf{q})(\mathbf{f}_T + \mathbf{f}_D)}{m} + \mathbf{g}, \quad (1b)$$

$$\dot{\mathbf{q}} = \frac{1}{2}\mathbf{q} \odot \begin{bmatrix} 0 \\ \boldsymbol{\omega} \end{bmatrix}, \quad (1c)$$

$$\dot{\boldsymbol{\omega}} = \mathbf{J}^{-1}(\boldsymbol{\tau} - \boldsymbol{\omega} \times \mathbf{J}\boldsymbol{\omega}), \quad (1d)$$

where the operator  $\odot$  denotes the quaternion multiplication,  $\mathbf{R}(\mathbf{q})$  is the rotational matrix of quaternion  $\mathbf{q}$ ,  $\mathbf{f}_T$  is the thrust vector in the body frame,  $\mathbf{f}_D$  is the drag force vector in the body frame,  $m$  is the mass of the UAV,  $\mathbf{g}$  is the gravitational acceleration,  $\mathbf{J}$  is the diagonal inertial matrix of the rigid body of the UAV, and  $\boldsymbol{\tau}$  is the torque produced in the body frame.

Drag force  $\mathbf{f}_D$  in (1) is usually modelled as a linear function of velocity in body frame  $v_B$  with drag coefficients

$(k_{vx}, k_{vy}, k_{vz})$  [24], and can be computed as

$$\mathbf{f}_D = -[k_{vx}v_{B,x} \ k_{vy}v_{B,y} \ k_{vz}v_{B,z}]^T. \quad (2)$$

The derivative of the state (1) can be calculated using the body thrust vector  $\mathbf{f}_T$  and  $\boldsymbol{\tau}$  from the motor force vector  $\mathbf{f}$  such that

$$\begin{aligned} \mathbf{f}_T &= [0 \ 0 \ T]^T, \\ \begin{bmatrix} T \\ \boldsymbol{\tau} \end{bmatrix} &= \begin{bmatrix} 1 & 1 & 1 & 1 \\ l/\sqrt{2} & -l/\sqrt{2} & -l/\sqrt{2} & l/\sqrt{2} \\ -l/\sqrt{2} & -l/\sqrt{2} & l/\sqrt{2} & l/\sqrt{2} \\ \kappa & -\kappa & \kappa & -\kappa \end{bmatrix} \mathbf{f}, \end{aligned} \quad (3)$$

where  $l$  is the arm length of the symmetric quadrotor frame, and  $\kappa$  is the motor torque constant.

#### B. Standard OCP/MPC formulation

The standard NMPC problem is formulated as an Optimal Control Problem (OCP) in discrete time where the goal is to minimize a cost function  $J$  over a finite horizon  $N$ , and therefore, the system dynamics are discretized and propagated using a numerical integrator such as Runge-Kutta 4th order method. The next state of the system can then be computed as  $\mathbf{x}_{k+1} = f_{RK4}(\mathbf{x}_k, \mathbf{u}_k)$ , where  $\mathbf{x}_k$  and  $\mathbf{u}_k$  are the state and the input at time step  $k$ , respectively, and derivative of the state for each step is computed using the dynamics (1).

The NMPC problem is then formulated as

$$\min_{\mathbf{u}_0, \dots, \mathbf{u}_N} J(\mathbf{x}, \mathbf{u}) = \sum_{k=1}^{N-1} \tilde{\mathbf{x}}_k^T \mathbf{Q} \tilde{\mathbf{x}}_k + \sum_{k=0}^{N-1} \mathbf{u}_k^T \mathbf{R} \mathbf{u}_k + \tilde{\mathbf{x}}_N^T \mathbf{T} \tilde{\mathbf{x}}_N$$

subject to :

$$\begin{aligned} \tilde{\mathbf{x}}_k &= \mathbf{x}_k^* - \mathbf{x}_k, \quad \mathbf{x}_{k+1} = f_{RK4}(\mathbf{x}_k, \mathbf{u}_k), \\ \mathbf{x}_0 &= \mathbf{x}_{initial}, \quad \mathbf{u}_0 = \mathbf{u}_{initial}, \\ \mathbf{u}_k &\in [\mathbf{u}_{min}, \mathbf{u}_{max}], \quad \boldsymbol{\omega}_k \in [\boldsymbol{\omega}_{min}, \boldsymbol{\omega}_{max}], \end{aligned} \quad (4)$$

where  $[\bullet]_k$  is the quantity at  $t = t_{initial} + k\Delta t$ ,  $\tilde{\mathbf{x}}_k$  is the error in the state,  $\mathbf{x}_k^*$  is the desired state,  $N$  is the prediction horizon,  $\mathbf{Q}$  and  $\mathbf{R}$  are the penalty matrices for the state and input respectively,  $\mathbf{T}$  is the terminal penalty matrix,  $\mathbf{u}_{min}$  and  $\mathbf{u}_{max}$  are the control input limits to prevent actuator saturation, and  $\boldsymbol{\omega}_{min}$  and  $\boldsymbol{\omega}_{max}$  represent the limits imposed by state estimators on body rates of the aircraft. It is also important to note that the computation time of the OCP increases with the number of states, inputs, constraints, size of the prediction horizon, as well as the complexity of the dynamics model, and therefore, these quantities act as tuning parameters.

#### C. Choice of control inputs

As discussed in [16], the true physical limits of the system lie in the maximum torque produced by the motor for any given throttle  $t \in [0, 1]$ , and as the rotational speed of the motor increases, the increase in drag torque prevents further angular acceleration. It is due to this fact, that the rotational speed of the motor is modelled as a first-order system. When

torque produced by the drag force on the propellers is equal to the maximum torque of the motor, the propeller achieves its maximum rotational speed, and therefore, the maximum force of propulsion. This maximum force of propulsion along with the maximum torque produced by the motor defines the true physical limits of the propulsion system.

However, the control modality interface for the cascaded control architecture in commercial and research platforms is chosen to be the commanded collective thrust  $T_c$  and the desired body rates  $\omega_c$  as flight controllers firmwares such as PX4 and Betaflight expect these as inputs [11], [12]. For the NMPC, this desired control input can be calculated as part of the first predicted state ( $\omega_c = \omega_1$  from  $\mathbf{x}_0$ ) using (1d) and passed to the low-level controller as an input. Similarly, the desired collective thrust can be calculated as  $T_c = \sum_{i=1}^4 (f_{i,c})$  and passed to the low-level controller as an input. Owing to this, the control input for the NMPC itself is often virtual (non-real in physical sense) and can be chosen in many ways to facilitate modelling fidelity.

a) *First-order motor speed model*: When the motor dynamics are chosen to be modelled as a first-order system, the state can be expanded to  $\mathbf{x} = [\mathbf{p} \ \mathbf{q} \ \mathbf{v} \ \boldsymbol{\omega} \ \boldsymbol{\Omega}]^T$ , and the virtual control input  $\mathbf{u}$  can be chosen as the vector of commanded motor speeds  $\boldsymbol{\Omega}_c$ . The dynamics from (1) can be expanded with the dynamics of the motor as

$$\begin{aligned}\dot{\boldsymbol{\Omega}} &= \frac{1}{k_{mot}}(\boldsymbol{\Omega}_c - \boldsymbol{\Omega}), \\ \mathbf{f} &= c_f \boldsymbol{\Omega}^2,\end{aligned}\quad (5)$$

where  $k_{mot}$  is the time constant of the first-order motor dynamics, and  $c_f$  is the thrust coefficient of the propeller. Therefore,  $\mathbf{f}$  can be used to compute the body thrust vector  $\mathbf{f}_T$  and torque vector  $\boldsymbol{\tau}$  using (3), and the next state of the system can be obtained according to (1).

b) *First-order motor force model*: When the force produced by each motor is approximated as a first-order system instead, the virtual control input  $\mathbf{u}$  can be chosen as the vector of commanded motor forces  $\mathbf{f}_c$ , and the state can be modified as  $\mathbf{x} = [\mathbf{p} \ \mathbf{q} \ \mathbf{v} \ \boldsymbol{\omega} \ \mathbf{f}]^T$ . In this case, the dynamics of the motor forces can be computed as

$$\dot{\mathbf{f}} = \frac{1}{k_{mot,f}}(\mathbf{f}_c - \mathbf{f}), \quad (6)$$

where  $k_{mot,f}$  is the time constant of the first-order motor force dynamics, and (3) can be used to compute the body thrust vector and the torque vector. However, the force of the actuator is proportional to the square of rotational velocity of the propeller (5), and the approximation of actuator force to first-order system is inaccurate and causes loss of performance.

c) *No first-order modelling*: When first-order effects of the motor dynamics ((5) or (6)) are not considered, the virtual control input can be directly chosen as the commanded thrust vector  $\mathbf{f}_c$ , and therefore, (3) can be used to compute the body thrust vector and the torque vector.

d) *Problem of virtual inputs*: In a cascaded control architecture, the low-level controller is usually tasked with tracking the desired body rates and it utilizes the PID controller to generate the final commands to the actuators. Therefore, it is to be noted that none of the aforementioned choices of virtual inputs corresponds to the real input of the low-level controller, and the actual commanded throttles from the low-level controller to the motor controller are obtained through a linear map from the desired body rates to desired throttles as it passes through the PID controller. For example, in our testing, we found that the time taken by the body rates to reach their setpoint (as shown in Fig. 5) violates the assumption that the dynamics of the low-level controller are significantly faster than the high-level controller. Moreover, [26] showed that while choosing the actuator forces or actuator angular velocities as input reduces actuator saturation, conversion to torques and subsequent throttle commands during the mixing process in the low-level controller can cause actuator clipping and re-allocation of control near very-high or very-low throttle values. In these cases, it becomes imperative to devise a re-allocation and mixing strategy to prevent saturation and gain performance during agile manoeuvres. In conclusion, it can be stated that the dynamics of the low-level controller play a crucial role in the performance of the NMPC controller, and they cannot be neglected without loss of performance.

#### IV. PROPOSED LOL-NMPC METHODOLOGY

In this section, we propose a novel method which integrates the dynamics of the low-level controller into the high-level NMPC model to significantly improve the tracking performance of the UAV. The state of the UAV is augmented to include the integral error of the PID controller and the normalized angular velocities of the motors. We augment the model by including the PID dynamics in state space to formulate a new higher-fidelity model without substantially increasing the computational load of the controller. The input to the model is chosen as the collective desired throttle and the commanded body rates, which can directly command the low-level controller without causing actuator saturation or performance loss due to propagation of the desired body rates through the PID controller or NMPC model. As per the discussion in III-C, rotational velocity of the propeller  $\boldsymbol{\Omega}_i$  is a first-order system, and represents the true limit of the motors. Additionally, for any given propulsion setup, throttle and rotational velocity show a linear relationship such that  $f : [0, 1] \rightarrow [0, \Omega_{max}]$ . However, we amend this approach and propose an improvement in model fidelity by inculcating the dynamics of the low-level controller inside the model. First, we extend the state of the UAV such that

$$\mathbf{x}^{pid} = [\mathbf{p} \ \mathbf{q} \ \mathbf{v} \ \boldsymbol{\omega} \ \mathbf{z} \ \mathbf{r}]^T, \quad (7)$$

where  $\mathbf{z}$  is the integral error vector for PID in  $x$ ,  $y$ , and  $z$  axes,  $\mathbf{r}$  is the normalized angular velocity vector for each actuator. It is very important to note that since rotational velocity of the propeller and the applied throttle show a linear relationship for any given input voltage of a motor,

normalized angular velocity is equivalent to throttle ( $r \equiv t$ ), and therefore

$$\begin{aligned} r &= \frac{\Omega}{\Omega_{max}}, \\ \mathbf{f} &= f_{max}(\mathbf{r} \odot \mathbf{r}), \end{aligned} \quad (8)$$

where  $\odot$  denotes element-wise multiplication. The input to the model  $\mathbf{u}_{PID}$  is the collective desired throttle  $t_c$  and the commanded body rates  $\omega_c$  such that

$$\mathbf{u}^{pid} = [t_c \ \ \omega_c]^T. \quad (9)$$

We then model the PID dynamics in state space (as shown in [28]) such that

$$\begin{aligned} \mathbf{e} &= \omega_c - \omega, \\ \dot{\mathbf{z}} &= \mathbf{e}, \\ \tau_c &= k_p \mathbf{e} + k_i \mathbf{z} + k_d \dot{\mathbf{e}}, \end{aligned} \quad (10)$$

where  $\tau_c$  is the commanded torque vector produced by the modelled PID controller. However, instead of using  $k_d \dot{\mathbf{e}}$  term in (10), we use the preferred term  $k_d \dot{\omega}$ , which is not sensitive to change in commanded body rates  $\omega_c$ . For a traditional flight controller, the allocation of individual motor throttle ( $t$ ) from torques and collective throttle is performed using a mixer matrix  $\mathbf{G}$ , such that

$$\underbrace{\begin{bmatrix} t_{c,1} \\ t_{c,2} \\ t_{c,3} \\ t_{c,4} \end{bmatrix}}_{\tau_c \text{ or } \mathbf{r}_c} = \underbrace{\begin{bmatrix} 1 & -0.7071 & -0.7071 & -1.0 \\ 1 & 0.7071 & 0.7071 & -1.0 \\ 1 & -0.7071 & 0.7071 & 1.0 \\ 1 & 0.7071 & -0.7071 & 1.0 \end{bmatrix}}_{\mathbf{G}} \begin{bmatrix} t_c \\ \tau_c \end{bmatrix}. \quad (11)$$

We can then write the motor dynamics as

$$\dot{\mathbf{r}} = \frac{1}{k_{mot}}(\mathbf{r}_c - \mathbf{r}) \quad (12)$$

which we use inside the *LoL-NMPC* quadrotor model instead of the pure motor dynamics (5) to propagate the state to the next timestep.

*Constraints for LoL-NMPC:* In addition to low-level dynamics, as mentioned earlier in III-C and [26], the state-of-the-art suffers from a key issue near throttle limits where actuator clipping and control re-allocation can occur inside the mixer of the low-level controller and cause performance loss during agile manoeuvres. Our proposed formulation eliminates this key drawback by directly imposing linear constraints in the OCP solver in addition to the constraints discussed in III-B. Therefore, we can impose a linear constraint on the desired normalized angular velocity vector  $\mathbf{r}_c$  in (11) by expressing it as a function of  $\mathbf{x}^{pid}$  and  $\mathbf{u}^{pid}$ , such

that

$$\begin{aligned} \mathbf{r}_c &= \mathbf{G} \begin{bmatrix} t_c \\ \tau_c \end{bmatrix} = \mathbf{G} \begin{bmatrix} t_c \\ k_p(\omega_{cx} - \omega_x) \\ k_p(\omega_{cy} - \omega_y) \\ k_p(\omega_{cz} - \omega_z) \end{bmatrix} \\ &= \underbrace{\mathbf{G} \begin{bmatrix} 1 & 0 & 0 & 0 \\ 0 & k_{px} & 0 & 0 \\ 0 & 0 & k_{py} & 0 \\ 0 & 0 & 0 & k_{pz} \end{bmatrix}}_D \mathbf{u}^{pid} \\ &\quad - \underbrace{\mathbf{G} \begin{bmatrix} 0 & 0 & \dots & 0 & 0 & 0 & \dots & 0 \\ 0 & 0 & \dots & k_{px} & 0 & 0 & \dots & 0 \\ 0 & 0 & \dots & 0 & k_{py} & 0 & \dots & 0 \\ 0 & 0 & \dots & 0 & 0 & k_{pz} & \dots & 0 \end{bmatrix}}_C \mathbf{x}^{pid} \\ &\implies \mathbf{r}_c = \mathbf{C} \mathbf{x}^{pid} + \mathbf{D} \mathbf{u}^{pid}, \end{aligned} \quad (13)$$

and therefore, we can write the constraints on actuators as

$$\mathbf{r}_{min} \leq \mathbf{C} \mathbf{x}^{pid} + \mathbf{D} \mathbf{u}^{pid} \leq \mathbf{r}_{max}. \quad (14)$$

This constraint allows us to guarantee torque and thrust allocation in the mixer stage of the low-level controller and improve the performance of the high-level controller at platform limits.

## V. EXPERIMENTS AND RESULTS

In this section, we present the methodology and results of our extensive experiments conducted in simulated and real-world flights to validate the performance gained through our novel proposed *LoL-NMPC* formulation.

### A. Experimental Setup

For our simulation and real-world setup, we use a custom-built agile quadrotor measuring 300 mm diagonally (motor-to-motor) and weighing 1.2 kg. It is equipped with a CubePilot Cube Orange+ flight controller running PX4 firmware which acts as the low-level controller, and is commanded through our open-source MRS system architecture [29] running on a Khadas Vim3 Pro single-board computer. The UAV is powered by a 4S Lithium Polymer battery and propelled by a propulsion system capable of producing 80 Newtons of collective thrust at full throttle, and therefore the UAV has a thrust-to-weight ratio of  $\approx 7$ . For state estimation, the UAV is equipped with a Holybro F9P RTK GNSS module and receives real-time corrections from a base station, which are fused with the IMU onboard the flight controller to produce odometry for the system. To maintain parity between simulation and real-world experimental setup, the vehicle was tuned for high-agility and aggressive manoeuvres, and its step-response curve for body rates was measured in detail. The simulation and numerical modelling parameters were then tuned to match the real-world step-response curve of the model predictive controller. The results of this measurement and tuning are shown in Fig. 5, and we would like to highlight through this figure that the settling time of the low-level controller violates the fast dynamics assumption made in the state-of-the-art.

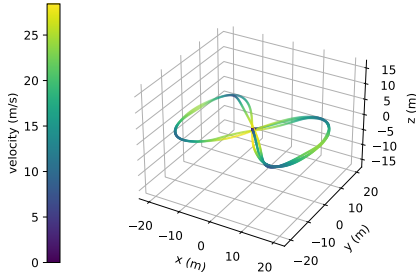


Figure 8 trajectory (fig 8).

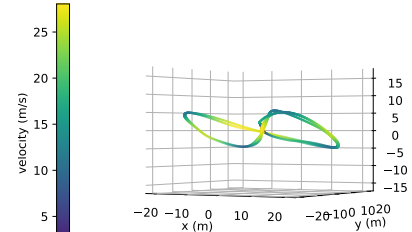
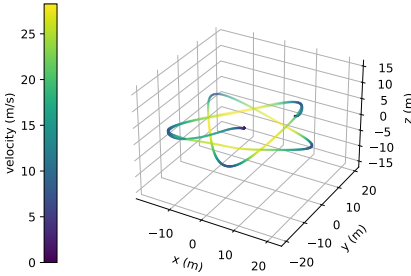


Figure 8 slanted trajectory (sl. fig 8).



Hypotrochoid trajectory (hyp.).

Fig. 2: Our three benchmark trajectories from CPC method [9] which were flown in the real-world.

## B. Experimental methodology

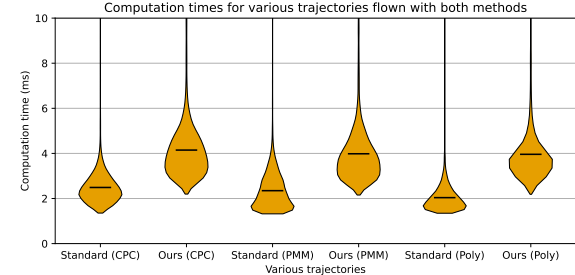
a) *Trajectory Generation*: It was shown in [13], that non-predictive controllers are sensitive to infeasible trajectories and how predictive controllers outperform them in tracking error on such trajectories. Therefore, we demonstrate the outstanding performance gains of our approach for three different types of trajectories.

- 1) CPC: Authors of [9] presented a time-optimal formulation for generation of feasible trajectories by incorporating actuator constraints and real physical parameters of the aircraft. While the method is computationally expensive, it produces near-time-optimal trajectories with high feasibility, and therefore, serves as a good benchmark for high-speed agile flight.
- 2) PMM: Current state-of-the-art in time-optimal point-mass trajectory generation was presented in [10]. Although point-mass trajectories have low-feasibility for aerial vehicles, it is important to include them for their non-smooth nature that can destabilise the non-linear optimisation for complex models inside the NMPC and therefore, they serve as a tough challenge for testing the limits of the platform. While these trajectories can be generated onboard the UAV in real-time, we use pre-generated trajectories for our experiments.
- 3) Polynomial: A computationally-efficient method for smooth and feasible polynomial trajectory generation was presented in [30]. These trajectories do not hold the UAV at its actuator saturation limits but provide a stable benchmark for all types of controllers.

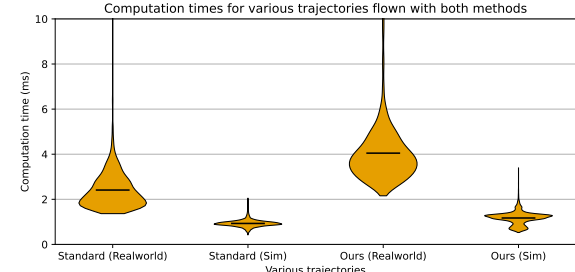
For our experiments, we chose to fly three different types of trajectories (Fig. 2), namely, the 8-figure trajectory (fig 8) for testing horizontal performance, the 8-figure slanted trajectory (sl. fig 8) for testing both horizontal and vertical performance, and the hypotrochoid trajectory (hyp.) for testing high-speed agile manoeuvres in tight-corners. Each of these trajectories was generated through the three aforementioned methods for both 2.5 g and 3.5 g accelerations, thereby producing 18 different trajectory comparisons.

b) *Testing parameters*: From here on, we use the term 'standard' to refer to the controller implemented using the standard dynamics in III-A, and the standard OCP formulation in III-B. We compare the performance of the standard controller with our proposed controller *LoL-NMPC* which uses the dynamics and constraints described in IV inside an OCP formulation described in III-B. We utilise

the Root Mean Square Error (RMSE) error from the desired trajectory as the primary performance metric for comparison of these controllers, and we also present the computation time statistics for both the simulation and real-world tests. For simulation tests, we use a direct emulation of our real-world platform and deploy it in Gazebo simulator with PX4 running as software-in-the-loop and the NMPCs running as part of our MRS architecture [29] on ROS1. For real-world tests, the platform was flown in the open-air in non-windy conditions, and over 170 flights were conducted to ensure error-free implementation of both the standard and our proposed controller. For both environments, the vehicle was limited to body rates of  $6 \text{ rad s}^{-1}$  in each axis and accelerations of  $4.0 \text{ g}$  to represent state estimator limits under civilian Global Navigation Satellite System (GNSS) use.



(a) Violin plot for computation time statistics and comparison for various trajectories in the real-world.

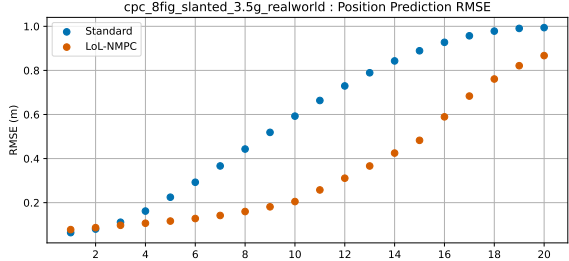


(b) Computation time comparison for flights in the real-world and simulations.

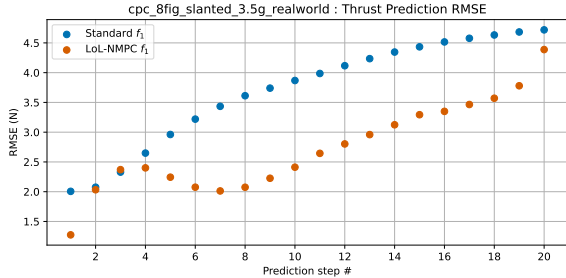
Fig. 3: Computation time statistics for simulations and real-world. The black bar marks the mean for each case.

## C. Simulation Results

a) *Computation time*: A primary requirement of high-speed agile manoeuvres is real-time decision making, and for this purpose, the high-level controller is expected to run at 100 Hz. The predictive controllers have been limited in



(a) Prediction performance in position for real-world tests.



(b) Prediction performance in thrust for real-world tests.

Fig. 4: Comparison between our proposed method and standard method for prediction of state in real-world tests.

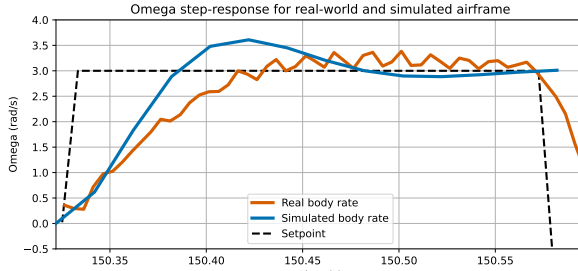


Fig. 5: Comparison of body rate response of the controller in simulation and in the real-world.

model fidelity due to this computation time limit of 10 ms, and through Fig. 3b, we show that our proposed model meets the requirement for computation limit both in a simulation on a workstation, but more importantly on an ARM-based onboard companion computer of the UAV.

*b) Tracking Error:* For simulation environment, we present the statistical analysis across 180 different flight tests conducted for each controller (10 flights per test case) through Table I. The RMSE error was calculated over each trajectory flown and the table Table I shows the mean and standard deviation of the RMSE error over 10 runs performed per trajectory per controller. The results clearly show the low variance and high stability in the performance of both controllers across all trajectories. Additionally, it can be seen that our proposed controller outperforms the standard controller by up to 29.16 % in tracking error, and offers an average gain of 22.31 % across all trajectories.

#### D. Real-world results

For the presentation of real-world RMSE results, we first tested the real-world variability of the results by conducting several flights with the slanted figure-8 trajectory at 3.5 g using both the CPC and PMM methods. The results showed

TABLE I: RMSE for trajectory tracking in simulations

type	trajectory	acc.	Standard (m)	ours (m)	gain (%)
CPC	fig 8	2.5g	0.456 ± 0.013	<b>0.370 ± 0.008</b>	18.85
CPC	fig 8	3.5g	0.662 ± 0.050	<b>0.477 ± 0.018</b>	27.94
CPC	sl. fig 8	2.5g	0.457 ± 0.007	<b>0.373 ± 0.011</b>	18.38
CPC	sl. fig 8	3.5g	0.650 ± 0.010	<b>0.489 ± 0.036</b>	24.76
CPC	hyp.	2.5g	0.441 ± 0.014	<b>0.384 ± 0.016</b>	12.92
CPC	hyp.	3.5g	0.577 ± 0.036	<b>0.472 ± 0.017</b>	18.19
PMM	fig 8	2.5g	0.393 ± 0.012	<b>0.321 ± 0.009</b>	18.32
PMM	fig 8	3.5g	0.538 ± 0.009	<b>0.422 ± 0.014</b>	21.56
PMM	sl. fig 8	2.5g	0.405 ± 0.010	<b>0.314 ± 0.008</b>	22.46
PMM	sl. fig 8	3.5g	0.567 ± 0.016	<b>0.437 ± 0.016</b>	22.92
PMM	hyp.	2.5g	0.401 ± 0.011	<b>0.322 ± 0.011</b>	19.70
PMM	hyp.	3.5g	0.551 ± 0.013	<b>0.433 ± 0.016</b>	21.41
Poly	fig 8	2.5g	0.210 ± 0.005	<b>0.153 ± 0.004</b>	27.14
Poly	fig 8	3.5g	0.300 ± 0.011	<b>0.226 ± 0.006</b>	24.66
Poly	sl. fig 8	2.5g	0.216 ± 0.008	<b>0.153 ± 0.007</b>	29.16
Poly	sl. fig 8	3.5g	0.299 ± 0.006	<b>0.224 ± 0.011</b>	25.08
Poly	hyp.	2.5g	0.209 ± 0.005	<b>0.150 ± 0.006</b>	28.22
Poly	hyp.	3.5g	0.271 ± 0.006	<b>0.217 ± 0.007</b>	19.92

a standard deviation of 0.1 m for CPC and 0.011 m for PMM, and therefore, we can conclude that the presented results are repeatable and show the true performance gained over the standard methods.

*a) Tracking Error:* Experimental results from the real-world flights are presented in Table II and show the RMSE tracking error for each trajectory in its own row, and for each controller in its column. The results indicate a clear performance improvement over the standard methodology with a maximum of 38.6 % gain in performance, and an average gain of 21.97 % across all trajectories. The average gain in performance matches the predicted gain from simulation experiments, thereby proving the reliability of the proposed testing methodology in both simulated and real-world environments.

*b) Prediction Error:* Given the results from the earlier section, we present a detailed look at how the performance gain can be quantified and studied further. For this purpose, we analyse the prediction performance of the controller to quantify the claimed higher fidelity offered by our proposed model inside the *LoL-NMPC*. For this analysis, the real-world data was interpolated to determine the timestamp closest to the predicted time step from every instance of the NMPC flight, and Fig. 4a and Fig. 4b show the RMSE of predictions made for position and thrust, respectively. As seen in Fig. 4a, our proposed model is able to predict the position of the aircraft within an error of 0.2 m at the 10th prediction step compared to a three-times worse prediction error of 0.6 m for the standard controller. Similarly, Fig. 4b shows the clear advantage in prediction performance for actuator force during trajectory tracking, which arises from the novel actuator modelling inside our model.

## VI. CONCLUSION

In this paper, we presented a novel formulation for a NMPC which integrates the usually-neglected low-level controller dynamics in addition to drag and actuator dynamics. Using this approach, we eliminate the need for a separate control re-allocation and mixing strategy for agile manoeuvres performed at throttle limits. Our proposed formulation allows the UAV to perform agile manoeuvres at very high

TABLE II: RMSE for trajectory tracking in real-world

type	trajectory	acc.	Standard (m)	ours (m)	gain (%)	max v (m/s)
CPC	fig 8	3.5g	0.931	<b>0.740</b>	20.530	26.666
CPC	fig 8	2.5g	0.647	<b>0.517</b>	20.130	22.051
CPC	sl. fig 8	3.5g	1.261	<b>1.046</b>	17.069	26.154
CPC	sl. fig 8	2.5g	0.818	<b>0.568</b>	30.577	22.173
CPC	hyp.	3.5g	<b>0.783</b>	0.813	-3.767	27.381
CPC	hyp.	2.5g	0.501	<b>0.464</b>	7.429	22.522
PMM	fig 8	3.5g	0.797	<b>0.575</b>	27.884	25.468
PMM	fig 8	2.5g	0.456	<b>0.385</b>	15.551	20.587
PMM	sl. fig 8	3.5g	1.018	<b>0.726</b>	28.645	23.286
PMM	sl. fig 8	2.5g	0.675	<b>0.640</b>	5.251	20.766
PMM	hyp.	3.5g	0.846	<b>0.566</b>	33.086	24.993
PMM	hyp.	2.5g	0.480	<b>0.331</b>	30.904	20.237
Poly	fig 8	3.5g	0.665	<b>0.420</b>	36.871	17.276
Poly	fig 8	2.5g	0.510	<b>0.481</b>	5.649	13.821
Poly	sl. fig 8	3.5g	0.629	<b>0.460</b>	26.783	17.692
Poly	sl. fig 8	2.5g	0.564	<b>0.346</b>	38.609	14.120
Poly	hyp.	3.5g	0.465	<b>0.345</b>	25.718	14.685
Poly	hyp.	2.5g	0.389	<b>0.278</b>	28.541	11.798

speeds without compromising tracking performance at accelerations of upto 3.5 g. Through extensive validation and testing with over 350 flights in simulated and real-world environment, we demonstrate an average performance gain of  $\approx 22\%$ , and a maximum performance gain of  $\approx 38\%$  in tracking error over the standard methodology in the real-world without external state estimators. Our method remains computationally feasible while offering a significant uplift in performance over the standard method in every scenario.

## REFERENCES

- [1] P. Rudol and P. Doherty, "Human body detection and geolocalization for uav search and rescue missions using color and thermal imagery," in *2008 IEEE Aerospace Conference*, 2008, pp. 1–8.
- [2] D. Kingston, R. W. Beard, and R. S. Holt, "Decentralized perimeter surveillance using a team of uavs," *IEEE Transactions on Robotics*, vol. 24, no. 6, pp. 1394–1404, 2008.
- [3] J. Han and Y. Chen, "Multiple uav formations for cooperative source seeking and contour mapping of a radiative signal field," *Journal of Intelligent & Robotic Systems*, vol. 74, no. 1, pp. 323–332, Apr 2014.
- [4] P. Štibinger, T. Báča, and M. Saska, "Localization of ionizing radiation sources by cooperating micro aerial vehicles with pixel detectors in real-time," *IEEE Robotics and Automation Letters*, vol. 5, no. 2, pp. 3634–3641, 2020.
- [5] M. Burri, J. Nikolic, C. Hürzeler, G. Caprari, and R. Siegwart, "Aerial service robots for visual inspection of thermal power plant boiler systems," in *2nd International Conference on Applied Robotics for the Power Industry*, 2012, pp. 70–75.
- [6] T. Merz and F. Kendoul, "Beyond visual range obstacle avoidance and infrastructure inspection by an autonomous helicopter," in *IEEE/RSJ International Conference on Intelligent Robots and Systems*, 2011, pp. 4953–4960.
- [7] D. Datsko, F. Nekovar, R. Penicka, and M. Saska, "Energy-aware multi-uav coverage mission planning with optimal speed of flight," *IEEE Robotics and Automation Letters*, vol. 9, no. 3, pp. 2893–2900, 2024.
- [8] D. Hanover, A. Loquercio, L. Bauersfeld, A. Romero, R. Penicka, Y. Song, G. Cioffi, E. Kaufmann, and D. Scaramuzza, "Autonomous drone racing: A survey," *IEEE Transactions on Robotics*, vol. 40, pp. 3044–3067, 2024.
- [9] P. Foehn, A. Romero, and D. Scaramuzza, "Time-optimal planning for quadrotor waypoint flight," *Science Robotics*, vol. 6, no. 56, p. eabhl221, July 2021.
- [10] K. Teissing, M. Novosad, R. Penicka, and M. Saska, "Real-time planning of minimum-time trajectories for agile uav flight," *IEEE Robotics and Automation Letters*, vol. 9, no. 11, pp. 10351–10358, 2024.
- [11] P. Foehn, E. Kaufmann, A. Romero, R. Penicka, S. Sun, L. Bauersfeld, T. Laengle, G. Cioffi, Y. Song, A. Loquercio, et al., "Agilicious: Open-source and open-hardware agile quadrotor for vision-based flight," *Science robotics*, vol. 7, no. 67, p. eabl6259, 2022.
- [12] D. Hert, T. Baca, P. Petracek, V. Kratky, V. Spurny, M. Petrik, M. Vrba, D. Zaitlik, P. Stoudek, V. Walter, P. Stepan, J. Horyna, V. Pritzl, G. Silano, D. Bonilla Licea, P. Stibinger, R. Penicka, T. Nascimento, and M. Saska, "Mrs modular uav hardware platforms for supporting research in real-world outdoor and indoor environments," in *2022 International Conference on Unmanned Aircraft Systems (ICUAS)*, 2022, pp. 1264–1273.
- [13] S. Sun, A. Romero, P. Foehn, E. Kaufmann, and D. Scaramuzza, "A comparative study of nonlinear mpc and differential-flatness-based control for quadrotor agile flight," *IEEE Transactions on Robotics*, vol. 38, no. 6, pp. 3357–3373, 2022.
- [14] H. Nguyen, M. Kamel, K. Alexis, and R. Siegwart, "Model Predictive Control for Micro Aerial Vehicles: A Survey," in *2021 European Control Conference (ECC)*. Delft, Netherlands: IEEE, June 2021, pp. 1556–1563.
- [15] T. Lee, M. Leok, and N. H. McClamroch, "Geometric tracking control of a quadrotor uav for extreme maneuverability," *IFAC Proceedings Volumes*, vol. 44, no. 1, pp. 6337–6342, 2011.
- [16] D. Bicego, J. Mazzetto, R. Carli, M. Farina, and A. Franchi, "Nonlinear model predictive control with enhanced actuator model for multirotor aerial vehicles with generic designs," vol. 100, no. 3, pp. 1213–1247, 2020.
- [17] D. Hanover, P. Foehn, S. Sun, E. Kaufmann, and D. Scaramuzza, "Performance, Precision, and Payloads: Adaptive Nonlinear MPC for Quadrotors," *IEEE Robotics and Automation Letters*, vol. 7, no. 2, pp. 690–697, Apr. 2022.
- [18] Y. Chen, M. Brussetta, E. Picotti, and A. Beghi, "Matmpc - a matlab based toolbox for real-time nonlinear model predictive control," in *2019 18th European Control Conference (ECC)*, 2019, pp. 3365–3370.
- [19] R. Verschueren, G. Frison, D. Kouzoupias, J. Frey, N. van Duijkeren, A. Zanelli, B. Novoselnik, T. Albin, R. Quirynen, and M. Diehl, "acados - a modular open-source framework for fast embedded optimal control," *Mathematical Programming Computation*, 2021.
- [20] J. A. E. Andersson, J. Gillis, G. Horn, J. B. Rawlings, and M. Diehl, "CasADi – A software framework for nonlinear optimization and optimal control," *Mathematical Programming Computation*, vol. 11, no. 1, pp. 1–36, 2019.
- [21] D. Mellinger and V. Kumar, "Minimum snap trajectory generation and control for quadrotors," in *2011 IEEE international conference on robotics and automation*, pp. 2520–2525.
- [22] J. Svacha, K. Mohta, and V. Kumar, "Improving quadrotor trajectory tracking by compensating for aerodynamic effects," in *2017 International Conference on Unmanned Aircraft Systems*, pp. 860–866.
- [23] R. Mahony, V. Kumar, and P. Corke, "Multirotor aerial vehicles: Modeling, estimation, and control of quadrotor," *IEEE robotics & automation magazine*, vol. 19, no. 3, pp. 20–32.
- [24] M. Faessler, A. Franchi, and D. Scaramuzza, "Differential flatness of quadrotor dynamics subject to rotor drag for accurate tracking of high-speed trajectories," *IEEE Robotics and Automation Letters*, vol. 3, no. 2, pp. 620–626, 2018.
- [25] L. Bauersfeld\*, E. Kaufmann\*, P. Foehn, S. Sun, and D. Scaramuzza, "NeuroBEM: Hybrid aerodynamic quadrotor model," in *Robotics: Science and Systems XVII*. Robotics: Science and Systems Foundation, 2021.
- [26] M. Faessler, D. Falanga, and D. Scaramuzza, "Thrust mixing, saturation, and body-rate control for accurate aggressive quadrotor flight," *IEEE Robotics and Automation Letters*, vol. 2, no. 2, pp. 476–482, 2017.
- [27] E. Tal and S. Karaman, "Accurate Tracking of Aggressive Quadrotor Trajectories Using Incremental Nonlinear Dynamic Inversion and Differential Flatness," *IEEE Transactions on Control Systems and Technology*, vol. 29, no. 3, pp. 1203–1218, 2020.
- [28] W. Tan, W. Han, and J. Xu, "State-space pid: A missing link between classical and modern control," *IEEE Access*, vol. 10, pp. 116540–116553, 2022.
- [29] T. Baca, M. Petrik, M. Vrba, V. Spurny, R. Penicka, D. Hert, and M. Saska, "The mrs uav system: Pushing the frontiers of reproducible research, real-world deployment, and education with autonomous unmanned aerial vehicles," *Journal of Intelligent & Robotic Systems*, vol. 102, no. 1, Apr. 2021.
- [30] Z. Wang, H. Ye, C. Xu, and F. Gao, "Generating large-scale trajectories efficiently using double descriptions of polynomials," in *IEEE International Conference on Robotics and Automation*. Xi'an, China: IEEE, 2021, pp. 7436–7442.